Proof-of-Concept for a Ground-Based Dual-Receiver Radar Architecture to Estimate Snowpack Parameters for Wet Snow

Pedro Fidel Espín-López, Martina Lodigiani, *Student* Member, IEEE, Massimiliano Barbolini, Fabio Dell'Acqua, *Senior Member*, *IEEE*, Lorenzo Silvestri, *Member*, *IEEE*, Marco Pasian, *Senior Member*, *IEEE*

***Abstract* — Snow is an important environmental variable and a primary water resource in many areas of the world. Monitoring seasonal snowpack properties is also crucial for properly managing snow-related hazards such as snow avalanches and snowmelt floods. Recently, an innovative radar architecture, based on the use of two receivers, has been proposed for snowpack monitoring for the case of dry snow, where the snowpack depth and bulk density can be calculated with one single radar measurement, without any kind of external aid.**

This paper presents the extension of this innovative radar architecture for the case of wet snow. The approach to determine, not only the snowpack depth and bulk density, but also the liquid water content, is outlined and discussed in detail, along with the experimental validation of the operating principle for two cases.

***Index Terms* — Downward-looking radar, FMCW radar, liquid water content (LWC), snowpack, snow density, snow monitoring, snow water equivalent (SWE), wave speed, wet snow.**

I. Introduction

SNOW COVER is an important variable of the climate system and represents a vital storage of freshwater [1]. On the other hand, it may also play a major role in natural disasters such as snow avalanches and floods [2], [3]. To model the snowpack, even for wet snow, information on snow depth (*HS*), snow density (ρ_s), volumetric liquid water content (*LWC*), and snow water equivalent (*SWE*) are necessary inputs [4]. In particular, it can be worth observing that *SWE* can be defined either as [4]:

$$SWE = HS\ \rho_s \tag{1}$$

measured in millimetres of water equivalent (mm w.e.) or in kilograms per square meter (kg m^{-2}). Alternatively, it may be defined as [5]:

$$SWE = HS\ \rho_s / \rho_w \tag{2}$$

measured in millimetres (mm), where ρ_w is the water density (1000 kg/m^3). This second definition is used in this paper.

HS, ρ_s, and *LWC* are important indicators for snow stability. In particular, for wet snow, *LWC* has a crucial impact in wet-snow avalanche prediction [2], [6], as well as for the onset of meltwater run-off [7]–[9], and for what concerns the modelling of the climate system, the albedo [10]. *SWE* is a critical parameter for the reservoirs of hydro-power stations, for hydrological models, and in general for several water use applications [11], [12].

Microwave radars represent a valuable approach to monitor the snowpack, both for remote-sensing platforms, most notably satellites [13], [14], and for ground-based measurements, even for wet snow [15]–[18]. A common limitation for standard ground-based radars is that they cannot determine simultaneously the snowpack depth and the dielectric properties (hence, the physical properties) with a single radar measurement. For this reason, ground-based radars can be complemented in such a way that one or more physical parameters are provided otherwise. In particular, these are calculated on the grounds of a-priori assumptions measured by other means (e.g., ultrasonic and laser gauges, or water content reflectometers), or using a combination of radars and GPS receivers [17]–[20]. In other cases, different implementations based on multiple radar measurements are used, in order to achieve a solution relying only on radar signals. These implementations include electromechanical positioning enabling synthetic aperture radar tomography [21]–[24], and implementations under the general domain of the inverse-scattering, migration-focusing, common-offset, and common-mid-points techniques, often with radars mounted on snow-mobiles [25]–[31].

However, a-priori assumptions can be prone to large uncertainties. Additional devices other than radar increase the complexity of the system, in some cases still retain potentially large uncertainties, and/or require installations above the ground of some components not intended for rapid removal, making them unsuitable for portable measuring systems.

This work was partially supported by the Italian Ministry of Education, University and Scientific Research (MIUR) under the project SIR2014 "SNOWAVE" RBSI148WE5.

P. F. Espín-López was with the Department of Electrical, Computer and Biomedical Engineering, University of Pavia, Pavia, Italy (e-mail: pedrofidel.espinlopez01@universitadipavia.it). Now, he is with the Geomatics Division, Centre Tecnològic de Telecomunicacions de Catalunya (CTTC), Castelldefels, Spain.

M. Lodigiani, F. Dell'Acqua, L. Silvestri, and M. Pasian, are with the Department of Electrical, Computer and Biomedical Engineering, University of Pavia, Pavia, Italy (e-mail: martina.lodigiani01@universitadipavia.it; {fabio.dellacqua, lorenzo.silvestri, marco.pasian}@unipv.it).

M. Barbolini is with the Department of Civil Engineering and Architecure, University of Pavia, Pavia, Italy and with Flow-Ing s.r.l., La Spezia, Italy (email: massimiliano.barbolini@unipv.it; m.barbolini@flow-ing.com).

Finally, techniques based on classic multiple radar measurements, offering good accuracy in some cases, may suffer from the nonlinearity of the inversion process (e.g., local minima), the need for fortuitously located diffractors (e.g., rocks), the presence of artefacts, and the inconveniences of positioners, snow-mobiles, and sleds, if used. In addition, they normally require a large number of different radar offsets to get a good accuracy, but at the cost of a more complex measurement setup.

Recently, a different radar system, based on a novel dual-receiver, stand-alone, frequency-modulated continuous wave (FMCW) radar architecture, was presented for the case of dry snow [32]–[34]. For the first time, it was demonstrated the possibility to measure, at the same time, the snowpack depth *HS* and the wave speed into the snowpack (thus, the snowpack density ρ_s and *SWE*) with only two radar measurements, thus with a very simple, compact, and light system, particularly suitable for portable applications. It is worth observing that a system easy to be portable, is a key point to enhance the possibility of obtaining a more detailed spatial representativeness of the snowpack.

In this paper, it is presented the mathematical approach, along with the experimental verification of the operating principle, for two cases of wet snow. For wet snow, one more variable must be determined, *LWC*. This requires the development of a new set of equations, and to consider the cross-correlation between the complex dielectric permittivity of the snow and the physical parameters ρ_s and *SWE*. In particular, for wet snow, not only the times of flight, but also the differential power collected by the two receivers, are considered. In addition, a study on the achievable accuracy is presented.

This paper is organized as follows. Sec. II discusses the dielectric properties of wet snow, while Sec. III presents the proposed innovative radar architecture for snowpack monitoring in case of wet snow. Then, Sec. IV reports the experimental validation of the operating principle, and Sec. V is related to a discussion about the accuracy of the results.

II. Dielectric Properties of Wet Snow

At the frequencies of interest for this work, in the S band, the snow can be characterized using both the real (ε') and the imaginary parts (ε'') of the relative dielectric permittivity (the former is also known as dielectric constant). These are functions of both snow density and *LWC*. According to [35], in the case of wet snow:

$$\varepsilon' = 1 + A + B + C / (1+ (f / f_0)^2) \quad (3)$$

$$A = 1.83\ 10^{-3}\ \rho_{ds} \quad (3a)$$

$$B = 0.02\ LWC^{1.015} \quad (3b)$$

$$C = 0.073\ LWC^{1.31} \quad (3c)$$

$$\varepsilon'' = 0.073\ LWC^{1.31}\ (f / f_0) / (1+ (f / f_0)^2) \quad (4)$$

where ρ_{ds} is the dry snow density, measured in kg/m^3, f is the operative frequency, f_0 the relaxation frequency (around 9.07 GHz), and *LWC* is measured in volume percentage. It may be worth observing that for wet snow, the dry snow density ρ_{ds} can be derived according to:

$$\rho_s = \rho_{ds} + \rho_w\ LWC \quad (5)$$

In general, it can be observed that for wet snow a dependence on frequency holds. However, for a wide range of densities and values of *LWC*, which cover practically all real-life cases, it can be observed that even if $\varepsilon'' > 0$, $\varepsilon'' << \varepsilon'$ for operating frequencies of a few GHz. Consequently, for both dry and wet snow, it is possible to apply an approximated relation between the speed v of the electromagnetic wave into the snowpack and ε' [36], indifferently for dry and wet snow:

$$v \sim c / \sqrt{\varepsilon'} \quad (6)$$

where c is the speed of light.

Then, it is interesting to observe that, in many practical cases, the knowledge of the dielectric constant ε', hence of the wave speed v, is sufficient to discriminate dry from wet snow. Indeed, normally the density for dry snow is rarely higher than around 450 kg/m^3, while moderately wet snow bulk densities often exceed this value, and can easily have a minimum *LWC* quantified in the order of 2-3%. Therefore, for these typical conditions, the dielectric permittivity, calculated, as an example, at 2.75 GHz, for dry snow is rarely higher than around 1.8 for the relative real part. Instead, for wet snow, the relative real part of the dielectric permittivity often exceeds two. Consequently, this may help to estimate whether the snow is dry or wet without further processing. This can be useful for some applications. For more complete calculation of the properties of the snow, including LWC, the approach is described in the subsequent Sec. III.

III. Radar Architecture for Wet Snow

The proposed dual-receiver radar architecture, operating principle, results, and possible enhancements, are discussed in [32]–[34], in case of dry snow. Here, the operating schema and the mathematical approach are extended for the case of wet snow. First, as anticipated in Sec. II, for dry and wet snow indifferently, the wave speed into the snowpack can be related to the real part of the relative dielectric permittivity, using (6). Thus, as presented in [34], using two independent propagation paths, the mathematical problem of determining both the snowpack depth *HS* and the wave speed v into the snowpack can be closed. This allows for explicitly deriving two independent equations for the snowpack thickness D (i.e., measured at right angle to the slope, thus immediately related to *HS* knowing the inclination of the slope) and the dielectric constant ε':

$$D^2 = (s_2^2\ T_1^2 - s_1^2\ T_2^2) / 4\ (T_2^2 - T_1^2) \quad (7)$$

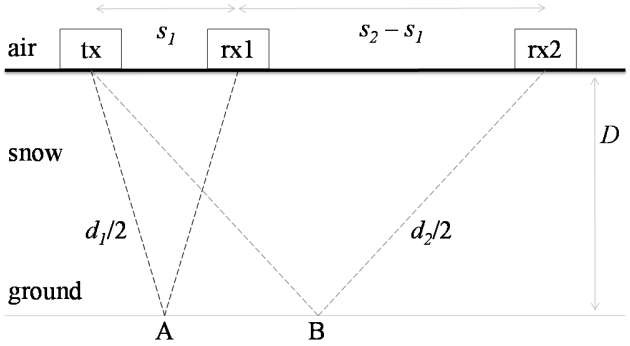

Figure 1: Radar architecture schema for the downward-looking configuration showing the transmitter (tx) and the two receivers (rx1 and rx2) installed above a snowpack with thickness D. The horizontal distance and the propagation distance are s_1 and d_1, respectively, for the first receiver, and s_2 and d_2, respectively, for the second receiver. Drawing not to scale.

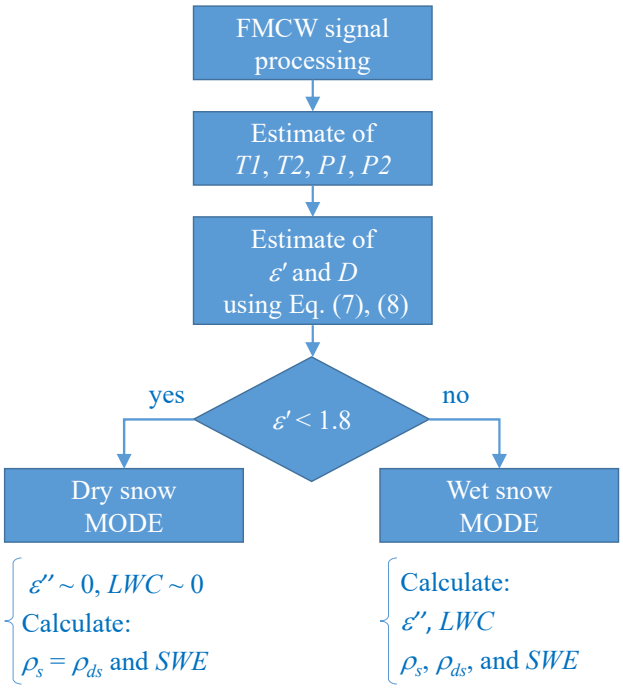

Figure 2: Work logic for the calculation of the snowpack parameters. $\varepsilon' = c^2$

$$(T_1 - T_2)(T_1 + T_2) / (s_1 - s_2)(s_2 + s_1) \quad (8)$$

where s_1, T_1, s_2, and T_2 are the ground distances and the times-of-flight between the transmitter and the first and second receiver, respectively (Fig. 1).

It is worth observing that the radar schema presented in [32]–[34], leveraging on the idea of multiple radar measurements, only makes use of two radar measurements. These latter are collected using two antennas [32], [34] or even one single antenna working on multi-path propagation [33]. Compared to other architectures using a larger number of multiple measurements, mentioned in Sec. I, this choice may return a sub-optimal result in terms of accuracy. However, the radar setups presented in [32]–[34], with only two radar measurements, aim at a portable, downward-looking, compact, and light system. These features are key benefits for several field applications where the radar is placed above the snow just for the time required for measuring, and then removed. In addition, for those cases where the average parameters of the snowpack are of interest, this sub-optimal accuracy can be partially offset by measuring the snowpack more than once at slightly different, adjacent locations, and then averaging the results, as demonstrated for dry snow in [34].

For wet snow, ε'' is to be determined. Taking advantage once more of the inequality $\varepsilon'' << \varepsilon'$, it is possible to correlate ε'' to the dissipation factor α_w due to the presence of liquid water [36]:

$$\alpha_w \sim (\pi \cdot f \cdot \varepsilon'') / \left(c \cdot \sqrt{\varepsilon'}\right) \quad (9)$$

Thus, once ε' is calculated using (8), and α_w is determined, it is possible to derive ε''. In order to experimentally measure α_w, a differential approach is adopted to minimize uncertainties. In particular, the power levels P_1 and P_2, detected respectively by the first and second receiver, can be related to the dissipation factor α_w using the radar equation [37]:

$$P_1 = P_t (G_1^2 \lambda^2 S_1) / ((4\pi)^3 d_1^4 L_1) \quad (10)$$

$$P_2 = P_t (G_2^2 \lambda^2 S_2) / ((4\pi)^3 d_2^4 L_2) \quad (11)$$

where P_t is the radiated power, G_1 and G_2 the antenna gains along the angular direction defined by the tx–rx_1 and tx–rx_2 paths, respectively, S_1 and S_2 are the radar cross sections at the end of the snowpack for the tx–rx_1 (point A in Fig. 1) and tx–rx_2 (point B in Fig. 1) paths, respectively, λ is the wavelength, d_1 and d_2 are the propagation distances from the transmitter to the first and second receiver, respectively. L_1 and L_2 are the loss values due to the dissipation factor α_w along the tx–rx_1 and tx–rx_2 paths, respectively. These latter can be calculated as:

$$L_1 = exp\,(2\, d_1\, \alpha_w) \quad (12)$$

$$L_2 = exp\,(2\, d_2\, \alpha_w) \quad (13)$$

Ideally, knowing the values assumed by all the parameters present either in (10) or (11), it would be possible to derive the dissipation factor α_w. However, this simple approach is prone to uncertainties. Indeed, the value of some parameters, for example the radiated power, is difficult to estimate (normal un-calibrated transmitters change their output power according to several working conditions, for example the ambient temperature, and the final radiated power is also affected by unpredictable reflections coming from the antenna-transmitter coupling and from the antenna-snow coupling). Instead, the differential comparison between P_1 and P_2 allows applying a more robust approach, where the absolute values of radiated power are disregarded:

$$P_1 / P_2 = (G_1^2 S_1 d_2^4 L_2) / (G_2^2 S_2 d_1^4 L_1) = \\ = (G_1^2 S_1 d_2^4) / (G_2^2 S_2 d_1^4) \exp (2 (d_2 - d_1) \alpha_w) \quad (14)$$

In (14) a direct relationship between the dissipation factor α_w and the ratio P_1 / P_2 between the power received at the first and second receiver is outlined. Indeed, G_1 and G_2 can be calculated analytically once the antennas are known, and S_1 and S_2 can be estimated using a formulation for the radar cross section in the near-field regime [38], [39]. At the same time, the differential approach allows for neglecting, in most practical cases, second-order corrections, for example related to the small variation in reflectivity with the incidence angle, as demonstrated with a practical example in Sec. IV.

Once both ε' and ε'' are determined, using (3) and (4) it is possible to calculate the dry snow density ρ_{ds} and liquid water content *LWC*. Consequently, using (7), (8), and (14), it is possible to have a simultaneous measurement of D (or HS), ρ_s, and *LWC*. The entire process in summarised in Fig. 2, where also the possibility to discriminate dry from wet snow just on the ground of the real part of the relative dielectric permittivity ε' is presented, as discussed in Sec. 2. However, the discrimination between dry and wet snow may be difficult in some cases, especially for values close to the threshold presented in Fig. 2 ($\varepsilon' < 1.8$). This is typically happening during the ripening phase of the melting, i.e., when the LWC is low and the wet front is just formed. In this case, it is still possible to apply a conservative approach, and solve the complete mathematical problem as if the snow was wet. Then, the appropriateness of this assumption can be evaluated a-posteriori in accordance with the values calculated for ε'' and *LWC*.

IV. Experimental Validation of the Operating Principle

The experimental test of the operating principle for the proposed radar architecture for wet snow took place in two separate test sites in the Italian Alps. The first experimental test was at an altitude of around 2500 m a.s.l. (45°40'10" N 7°18'30" E, 6 April 2017), and the second experimental test was at an altitude of around 2100 m a.s.l. (45°51'50" N 7°38'50" E, 7 May 2019). In both cases, the terrain is practically flat. The experimental set-up is shown in Fig. 3.

A metal rail is used to support the antennas, which are open-ended WR340 waveguides working from 2.2 to 3.3 GHz. These frequencies provide a reasonable compromise between penetration depth and resolution, for different snow conditions, dry (where the system was already presented [32]–[34]), and wet. The rail is placed in such a way it is parallel to the snowpack surface, normal to slope of the terrain. By experience, this is the condition that maximize the possibility that the rail is parallel to the terrain, which is unknown. The first antenna is used as transmitter, and the second antenna is manually translated along the rail in two different positions to simulate two independent receiving antennas at distances s_1 and s_2 from the transmitter. In particular, values ranging from 30 to 40 cm and from 60 to 70 cm are used for s_1 and s_2, respectively. This can be done because the target is basically static (i.e., no modifications to the composition of the snowpack) during the time required to collect these two measurements. This allows recording two independent radar profiles, as shown in Fig. 4, which are used to calculate the snowpack parameters as described in the previous sections. It is worth noting that a second-step version of the radar, conceptually identical, but with two physical receivers and a mechanical switch, is presented for dry snow in [34]. This simplifies the measurements, avoiding the care required to translate the antenna along the rail.

It is worth also noting that these values for s_1 and s_2 are selected to optimize the transportability of the system rather than the accuracy, which in general improves for larger values for s_1 and s_2, as described in detail in Sec. V. However, as these two experimental tests are aimed at the validation of the operating principle, a sub-optimum accuracy does not impair the demonstration.

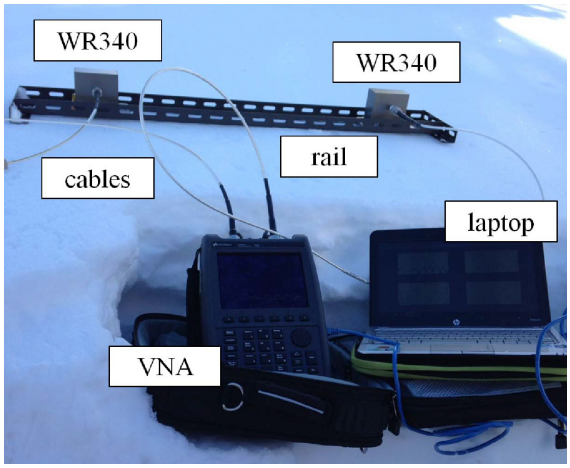

Figure 3: Experimental set-up for the experimental test.

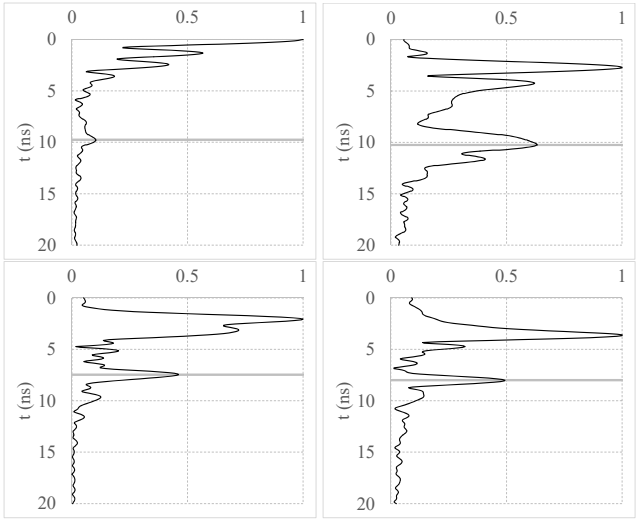

Figure 4: Radar profiles for the first test case (top) and the second test case (bottom). Normalized magnitude of the reflected signal for the first receiver (left) and the second receiver (right). In each profile the snow-ground interface is marked by a solid grey line.

Finally, the antenna coupling to the snow surface is maximized by the manual intervention of the operator, who physically places the radar above the snowpack as accurately as possible, aiming at a uniform contact between the antenna apertures and the snow surface. It may be interesting to observe that the radiation patterns of the antennas, when coupled directly to the snow, are different from the patterns of the case where they are allowed to radiate into the air. However, the antennas are not very directive, and the gain enhancement introduced by the direct coupling with the snow does not prevent proper operation of the system. This latter in fact requires the receiving antennas to pick up the signal reflected by the ground, generated by the transmitting antenna. Taking into account that the offsets between the antennas are short, less than 100 cm, this always guarantees in practice good mutual visibility within the reciprocal radiation patterns.

Looking at Fig. 4, several details can be appreciated. First, Fig. 4 shows the raw radar signals, as acquired by the receivers, without any kind of post-processing (which may be useful, for example, in view of semi-automatic routines, but at the same time may complicate the direct, intuitive, interpretation) but a normalization with respect to the magnitude of the highest peak. Some internal reflections, and the snow-ground interface, marked by a solid grey line, are visible. For example, for the first test case, the time-of-flight for the snow-ground interface is slightly less than 10 ns for the first receiver (approx. 9.75 ns), and slightly more than 10 ns for the second receiver (approx. 10.25 ns). Such a difference, approximately 0.5 ns, corresponding to around 15 cm of propagation in air, is in accordance with the system geometry, i.e., snowpack depth and distances between receivers.

The effect of a strong coupling, identified by a peak close to 0 ns, is visible for the first receiver of the first test case. The presence of this effect is strongly affected by local causes, mostly related to the snow-air discontinuity and antenna coupling to the snow. As anticipated previously in this same paragraph, these aspects may play an important role, but given the natural variability of the snow, and the manual operation of the radar, placed above the snowpack, the final effect in terms of coupling may be difficult to predict accurately. However, if present, this strong coupling is normally very far from the snow-ground interface, and does not jeopardize the correct interpretation of the latter.

The radar measurements are followed by a manual snowpack analysis, carried out by professional chartered AINEVA (Italian association for snow and avalanches) experts, according to the Italian standard procedure for manual snow profiling. The manual analysis is performed digging a snow pit ideally at the same location where the radar measurements took place. In particular, the depth is measured with a field ruler, with a maximum estimated error of ±1 cm. Bulk density is obtained probing with a sampler (volume 198 cm^3) and weighting with a dynamometer a series of snow samples of known volume taken from the different layers forming the snowpack. In this case, taking into account the resolution of the dynamometer, i.e. 1 g, and to be conservative a sampled volume inaccuracy of ±5%, the maximum error is around ±7%. Thus, combining the maximum estimated error for depth and density, it is possible to estimate the maximum estimated error for the *SWE* (calculated in accordance with (2), knowing the snowpack depth and density), which is approximately ±7% as well.

The per-layer *LWC* is determined in accordance with the classic test normally used for the manual analysis ("glove" test) of the snowpack (first test, [4]) or using the Finnish snow fork (second test, [40]), respectively. For the "glove" test, for the case of interest, the error is ±2.5%. For the second test, using the snow fork, the error is 0.5% [41]. The manual estimation of the *LWC* is a qualitative test, ideally not suitable for quantitative studies [41]. However, the "glove" test remains widely used for field operations [41]. For this reason, despite its poor accuracy, it still provides a qualitative comparison useful to contextualize the radar measurements within the framework of a widely accepted test for field operators. It is also worth observing that the *LWC* is a parameter possibly with large spatial differences, as the snowpack structure when wet snow is present can be complex [42]–[44]. This may lead to further inaccuracies, for example when the location of the manual analysis is not perfectly aligned with the location of the radar measurement. Finally, the maximum expected errors for all other parameters (ρ_{ds}, ε', v, and ε'') are directly calculated based on the errors for *HS*, ρ_s, *SWE*, and *LWC*.

For the first test, the results are summarized in Table I. Concerning the manual analysis, it is interesting to observe that in this case the *LWC* was measured manually [4], and it was found to be uniform over the entire snowpack, with a wetness index 3 (wet) for all layers. This means that the *LWC* can range from 3% to 8%, with an average of 5.5%. As anticipated, the poor accuracy for the *LWC* imposes large inaccuracies to the parameters ρ_{ds}, ε', v, and ε'', as it can be seen in Table I. In particular, the equivalent dry snow density ρ_{ds} ranges from 310 kg/m^3 (if *LWC* = 3%) to 216 kg/m^3 (if *LWC* = 8%), with an average of 263 kg/m^3 (if *LWC* = 5.5%). According to these measurements, the expected ε' ranges from 1.83 to 2.66 (average 2.22) and the expected wave speed v ranges from $2.22 \cdot 10^8$ m/s to $1.84 \cdot 10^8$ m/s (average $2.01 \cdot 10^8$ m/s). These values are calculated at 2.75 GHz (the central frequency of the radar system). It is interesting to observe that the variation of these parameters within the radar bandwidth (2.2 – 3.3 GHz) can be considered negligible (e.g., for the case ρ_{ds} = 263 kg/m^3 and LWC = 5.5%, ε' ranges from 2.24 to 2.20 at 2.2 GHz and 3.3 GHz, respectively). Finally, the expected ε'' ranges from 0.09 to 0.31 (average 0.19) at 2.75 GHz.

On the other side, the dual-receiver radar measurement provides *HS* = 0.98 m and $v = 1.99 \cdot 10^8$ m/s. Consequently, the calculated dielectric constant is $\varepsilon' = 2.27$. At the same time, the ratio P_1 / P_2 between the power received by the first receiver and the power received by the second receiver is around 3.53. Then, using (14) with $S_2/S_1 = 1.200$ and $G_1/G_2 = 1.318$ (calculated analytically according to [38], [39]; for comparison, the estimated difference in reflectivity at the snow-ground interface because of the different incidence angle

is approximately not larger than 1.05, thus validating the approximation presented at the end of Sec. III), it is calculated $\varepsilon'' = 0.16$ at 2.75 GHz. Solving (3) and (4) for the dry snow density and *LWC*, it is calculated $\rho_{ds} = 354$ kg/m^3 and *LWC* = 4.8%; this results in a bulk density $\rho_s = 402$ kg/m^3 and a *SWE* equal to 394 mm.

For the second test, the results are summarized in Table II. Concerning the manual analysis, it is interesting to observe that in this case the *LWC* was measured using the snow fork [40], sampling the snowpack with a step of 5 cm. This allowed for measuring with improved accuracy the bulk *LWC* for the entire snowpack (*LWC* = 3.75%). Then, even if the nominal accuracy is 0.5% [41], to account for an extra margin able to account for the difficulties of operating the snow fork in a real mountain scenario, an accuracy of 1% is account for. Nonetheless, the inaccuracies for the parameters ρ_{ds}, ε', v, and ε'' remain smaller compared to the first test, as it can be seen in Table II. In particular, the equivalent dry snow density ρ_{ds} ranges from 341 kg/m^3 (if *LWC* = 2.75%) to 277 kg/m^3 (if *LWC* = 4.75%), with an average of 309 kg/m^3 (if *LWC* = 3.75%). According to these measurements, the expected ε' ranges from 1.85 to 2.20 (average 2.02) and the expected wave speed v ranges from $2.02 \cdot 10^8$ m/s to $2.21 \cdot 10^8$ m/s (average $2.11 \cdot 10^8$ m/s). These values are calculated at 2.75 GHz Finally, the expected ε'' ranges from 0.08 to 0.16 (average 0.11) at 2.75 GHz.

TABLE I – RESULTS SUMMARY, TEST #1.

Parameter	Manual analysis	Radar measurement
HS	127 ± 1 cm	98 cm
ρ_s	318 ± 22 kg/m^3	402 kg/m^3
SWE	404 ± 31 mm	394 mm
LWC [4]	5.5 ± 2.5 %	4.8 %
ρ_{ds}	263 ± 47 kg/m^3	354 kg/m^3
ε'	2.22 (1.83–2.66)	2.27
v	2.01 (1.84–2.22) $\cdot 10^8$ m/s	$1.99 \cdot 10^8$ m/s
ε''	0.19 (0.09–0.31)	0.16

TABLE II – RESULTS SUMMARY, TEST #2.

Parameter	Manual analysis	Radar measurement
HS	82 ± 1 cm	76 cm
ρ_s	346 ± 24 kg/m^3	341 kg/m^3
SWE	284 ± 22 mm	258 mm
LWC [40]	3.75 ± 1 %	3.80 %
ρ_{ds}	309 ± 32 kg/m^3	303 kg/m^3
ε'	2.02 (1.85–2.20)	2.02
v	2.11 (2.02–2.21) $\cdot 10^8$ m/s	$2.11 \cdot 10^8$ m/s
ε''	0.11 (0.08–0.16)	0.12

The dual-receiver radar measurement provides *HS* = 0.76 m and $v = 2.11 \cdot 10^8$ m/s. Consequently, the calculated dielectric constant is $\varepsilon' = 2.02$. At the same time, the ratio P_1 / P_2 between the power received by the first receiver and the power received by the second receiver is around 2.11. Then, using again (14) with $S_2/S_1 = 1.200$ and $G_1/G_2 = 1.318$ (calculated analytically according to [38], [39]) it is calculated $\varepsilon'' = 0.12$ at 2.75 GHz. Solving (3) and (4) for the dry snow density and *LWC*, it is calculated $\rho_{ds} = 303$ kg/m^3 and *LWC* = 3.80%; this results in a bulk density $\rho_s = 341$ kg/m^3 and a *SWE* equal to 258 mm.

V. DISCUSSION ON THE ACCURACY OF THE RESULTS

The experimental results reported in the previous chapter account for the possibility for the proposed system to calculate important parameters for both dry and wet snowpacks. The best theoretical accuracy achievable for this calculation is primarily dictated by the accuracy achievable for the measurement of the times-of-flight T_1 and T_2. This is affected by a number of factors (e.g., sampling of the radar signal, antenna misalignments, uncorrected biases in the propagation within cables and antennas), but two of them are of primary importance, as discussed in the following.

First, the operating principle requires a flat snow/ground interface, as depicted in Fig. 1 (or ideally the knowledge of the shape of the terrain), to calculate the times of flight and the attenuations of the radar signal between the transmitter and the receivers. In real cases, however, as exemplified by our test sites, the unavoidable and unknown unevenness of the snow-ground interface inevitably determines an error in the measurement of the times of flights. As an example, for a typical case where $s_1 = 30$ cm, $s_2 = 70$ cm, *HS* = 100 cm, and $\varepsilon' = 1.5$, on a flat terrain the theoretical difference between d_1 and d_2 is around 9.66 cm, and the distance between the two reflection points at the snow/ground interface (points A and B in Fig. 1) is 20 cm ($s_2/2 - s_1/2$). This means that an unevenness of the terrain in the order of 1 cm between points A and B may cause an error in the measurement of the times of flight in the order of 10%, generally much larger than any other source of error. This problem, which is intrinsically random, can be usually mitigated by repeating the radar measurement a number of times, slightly changing the position of the radar above the surface of the snow, and averaging the results, as shown in [34]. It is worth observing that the radar architecture is based on deploying two independent receivers, which do not require external devices or references, other assumptions, or complex movements or post-processing. This makes possible to realize multiple measurements, for a single test site, in a matter of minutes, thus greatly mitigating any unevenness of the terrain.

The second important factor impacting on accuracy is the relative separation between the receivers and the transmitter. In particular, taking into account (7) and (8), the partial derivatives with respect to T_1 and T_2 can be calculated:

$$\delta D/D = Q1 / Q2 \tag{15}$$

$$Q1 = T_2 T_1 \delta t \{T_2 (s_2^2 - s_1^2) + T_1 (s_1^2 - s_2^2)\} \tag{15a}$$

$$Q2 = (T_2^2 - T_1^2)^2 \{s_2^2 T_1^2 - s_1^2 T_2^2\} \tag{15b}$$

$$\delta \varepsilon'/\varepsilon' = 2\delta t \{ T_1 + T_2 \} / |T_1^2 - T_2^2| \tag{16}$$

where δt is the error affecting the measurement of the times-of-flight. Now, to better understand how the geometry of the system, most notably s_1 and s_2, affects the results, (15) and (16) can be plotted for different values of s_1 and s_2 of interest in practical cases, from 0 to 1.5 m, and for different notable snowpacks with D = 1 m and ε' = 1.1, 1.4, 1.8, and 3.5, as shown in Fig. 5. This range of values for ε' is useful for addressing extreme conditions, from very dry snow to significantly wet snow. As an example, Fig. 5 is realized assuming:

$$\delta t = 1 / 2B \tag{17}$$

where B is the radar bandwidth. In this case δt would equal the radar resolution. This is not directly related to radar accuracy, but it is common practice to use it as a worst-case indication, as in all practical cases accuracy will be no worse than resolution. In this case, with a bandwidth B = 1.1 GHz, the δt is approximately 0.45 ns.

First, all cases in Fig. 5 look similar, thus showing no different trend for dry and wet snow. Then, it can be appreciated that when the value for s_1 approaches the value for s_2, both $\delta D/D$ and $\delta\varepsilon'/\varepsilon'$ reach very high values (please note that all points with values exceeding 100% were removed, in order to avoid saturating the colour scale). This corresponds to the cases where the separation between the two receivers is too small. This, in turn, means that the time of flight T_1 is very similar to the time of flight T_2. Therefore, since the difference between T_1 and T_2 is too small, any error on the time of flights would have a large relative impact on the calculation of the snowpack thickness D and dielectric constant ε'. Instead, it can be appreciated that both $\delta D/D$ and $\delta\varepsilon'/\varepsilon'$ decrease when the difference between s_1 and s_2 increases. This is because the difference between T_1 and T_2 increases, and any error on the time of flights would have a smaller relative impact on the calculation of the snowpack depth D and dielectric constant ε'.

It may be interesting to observe that for the experimental validation of the operating principle presented in Sec. IV, the radar architecture is intentionally implemented (s_1 = 30–40 cm, s_2 = 60–70 cm) to optimize the transportability of the system (mass, volume, complexity) rather than the accuracy. While this choice partially leads to non-optimized values for the measured errors, the demonstration of the mathematical approach and the operating principle described in Sec. III is not limited by this aspect. These two aspects combined can explain why in some cases the relative error shown in Sec. IV is not optimal. Most notably, for the first test case, a relative error of around 22% and 26% affects the measurement of the snowpack depth and density, respectively. On top of these aspects, it is also interesting to observe that a non-linear relationship between the different physical and electrical parameters of the snowpack holds.

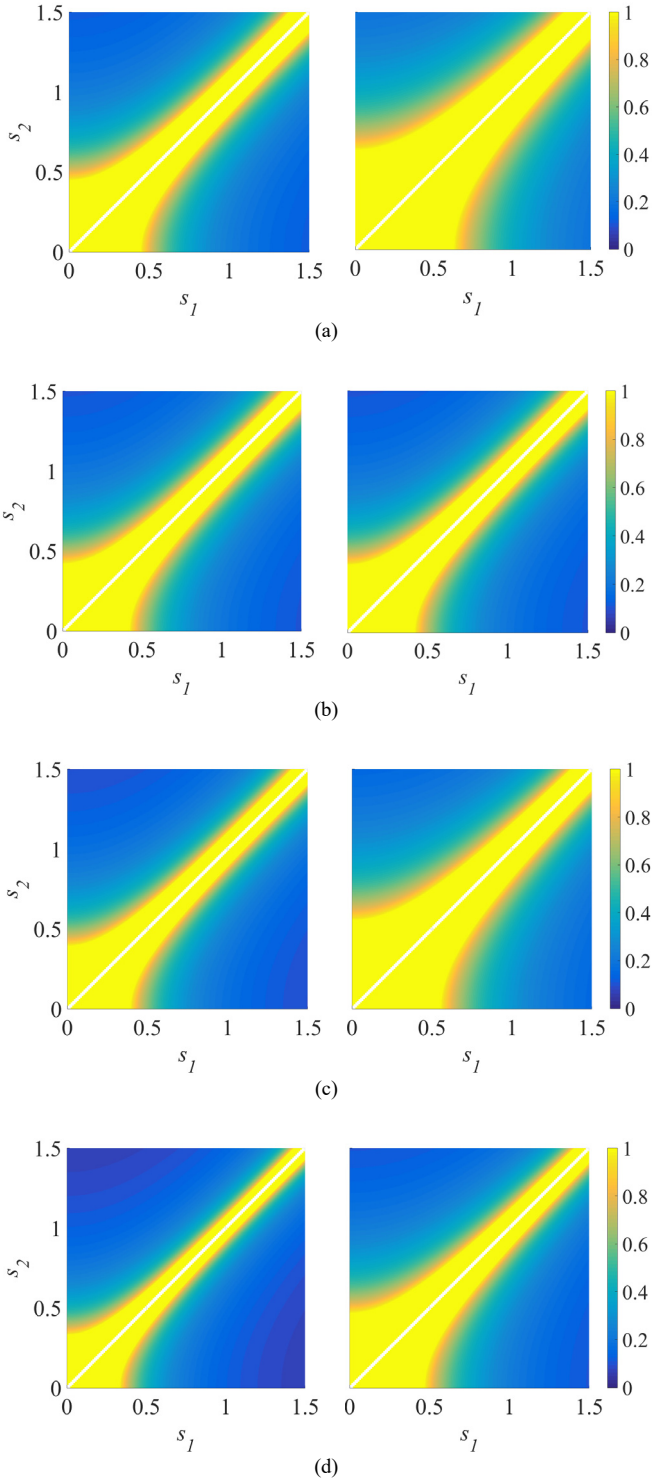

Figure 5: Maximum relative error for the calculation of the snowpack thickness (left) and dielectric constant (right) for different values of the parameters s_1 and s_2 (measured in meters) for a typical snowpack with a depth of one meter and a dielectric constant of: (a) 1.1; (b) 1.4; (c) 1.8; (d) 3.5. The colour scale ranges from 0% (0, dark blue) to 100% (1, bright yellow).

In addition, for wet snow, ε' and ε'' are determined jointly by both the *LWC* and ρ_s. This can generate a situation where comparatively small inaccuracies translate into large final errors. For example, for the first test case, if the measured *LWC* was 5.5% (instead of 4.8%), then the error on the snowpack density would improve from around 26% to around 8%.

Thus, while for optimized performance some mitigation strategies are desirable (e.g., larger values for s_1 and s_2, multiple measurements), the two tests cases demonstrated, even under sub-optimum conditions, the operating principle, and that the snowpack parameters can be measured even for wet snow.

VI. Conclusions

This paper presents experimental results for the demonstration of the operating principle for wet snow of a novel FMCW radar architecture for snowpack monitoring. This novel radar architecture, based on two receivers, can calculate the snowpack depth, bulk density, *LWC*, and *SWE*, with one single radar measurement of the times of flight between transmitter and receivers, and the differential power collected by the two receivers. The mathematical equations, used to solve the problem, are discussed, and the maximum expected errors are addressed, along with possible optimization strategies to reduce them. Two experimental test cases are presented to validate the operating principle.

However, further tests are required to assess the system under a larger variety of conditions, and better evaluate the response across different situations. It is also worth observing that, at the frequencies used for the proposed radar (S band), the maximum penetration of the radar signal within the wet snowpack should be evaluated carefully; the larger the *LWC*, the shorter the penetration depth, which could become insufficient to cover the snowpack depth. For example, when the dry snow density is 300 kg/m^3, and the *LWC* raises from 1% to 10%, the dissipation factor at 2.75 GHz increase from approx. 4 dB/m to approx. 28 dB/m. However, for seasonal snowpacks, higher *LWC* is normally related to snowpacks less thick, and this may lead to a partial compensation.

An open point remains the interpretation of the radar profile for each receiver, in particular the identification of the snow-ground interface. Semi- or fully-automatic routines are desirable, but their reliability should be verified against complex situations, where a number of factors, including internal reflections, spurious echoes, and non-optimized antenna coupling to the snow surface, can raise serious obstacles.

Finally, it is worth to point out that the proposed architecture represents the best solution in terms of compactness, cost, and mass, which are key features for portable instruments. Where portability is not the primary objective, alternatives using more than two receivers, and/or receivers further apart than the offsets considered here, may provide more accurate results.

Acknowledgements

The authors would like to thank *Fondazione Montagna Sicura – Montagne Sûre* and *Regione Autonoma Valle d'Aosta – Région Autonome Vallée d'Aoste* for their valuable support to the field activities, and the Finnish Meteorological Institute, in particular Leena Leppänen, for making the snow fork available.

References

[1] D. G. Vaughan, *et al*., *Observations: Cryosphere, Climate change 2013: The physical science basis*, Cambridge University Press, 2013.

[2] S. Baggi and J. Schweizer, "Characteristics of wet-snow avalanche activity: 20 years of observations from a high alpine valley (Dischma, Switzerland)," *Natur. Hazards*, Vol. 50, No 1, pp. 97–108, 2009.

[3] B. Bacchi and R. Ranzi, "Hydrological and meteorological aspects of floods in the Alps: an overview," *Hydrology and Earth System Sciences*, Vol. 7, No. 6, pp. 784–798, 2003.

[4] C. Fierz, *et al*., The International Classification for Seasonal Snow on the Ground. IHP-VII Technical Documents in Hydrology N°83, IACS Contribution N°1, UNESCO-IHP, Paris, 2009.

[5] M. Sturm, B. Taras, G. E. Liston, C. Derksen, T. Jonas, and J. Lea, "Estimating snow water equivalent using snow depth data and climate classes," *J. Hydrometeorology*, Vol. 11, pp. 1380–1394, 2010.

[6] C. Mitterer, H. Hirashima, and J. Schweizer, "Wet-snow instabilities: comparison of measured and modelled liquid water content and snow stratigraphy," *Ann. Glaciol*., Vol. 52, No. 58, pp. 201–208, 2011.

[7] S. Thompson, B. Kulessa, R. L. H. Essery, and M. P. Lüthi, "Bulk meltwater flow and liquid water content of snowpacks mapped using the electrical self-potential (SP) method," *The Cryosphere*, Vol. 10, pp. 433–444, 2016.

[8] C. Marin, G. Bertoldi, V. Premier, M. Callegari, C. Brida, K. Hürkamp, J. Tschiersch, M. Zebisch, and C. Notarnicola, "Use of Sentinel-1 radar observations to evaluate snowmelt dynamics in alpine regions," *The Cryosphere*, Vol. 14, pp. 935–956, 2020.

[9] M. Pasian, P. F. Espín-López, V. Premier, C. Notarnicola, C. Marin., "Identification of multi-temporal snow melting patterns with microwave radars," *2020 14th European Conference on Antennas and Propagation (EuCAP2019)*, Copenhagen, Denmark, March 15 – 20, 2020.

[10] T. P. Barnett, J. C. Adam, and D. P. Lettenmaier, "Potential impacts of a warming climate on water availability in snow-dominated regions," *Nature*, Vol. 438, pp. 303–309, 2005.

[11] F. Koch, M. Prasch, H. Bach, W. Mauser, F. Appel, and M. Weber, "How will hydroelectric power generation develop under climate change scenarios? A case study in the upper Danube basin," *Energies*, Vol. 4, pp. 1508–1541, 2011.

[12] W. Mauser and H. Bach, "PROMET – Large scale distributed hydrological modelling to study the impact of climate change on the water flows of mountain watersheds," *J. Hydrol*., Vol. 376, pp. 362–377, 2009.

[13] J. Shi, J. Dozier, J. and H. Rott, "Snow mapping in alpine regions with synthetic aperture radar," *IEEE Transactions on Geoscience and Remote Sensing*, Vol. 32, No. 1, pp. 152–158, 1994.

[14] H. Lievens, *et al*, "Snow depth variability in the Northern Hemisphere mountains observed from space." *Nature Communications*, Vol. 10, 2019.

[15] H. Gubler and M. Hiller, "The use of microwave FMCW radar in snow and avalanche research," *Cold Regions Science and Technology*, Vol 9, pp. 109–119, 1984.

[16] H.-P. Marshall and G. Koh, "FMCW Radars for snow research," *Cold Regions Science and Technology*, Vol. 52, pp. 118–131, 2008.

[17] C. Mitterer, A. Heilig, J. Schweizer, and O. Eisen, "Upward-looking ground-penetrating radar for measuring wet-snow properties," *Cold Regions Science and Technology*, Vol. 69, pp. 129–138, 2011.

[18] A. Heilig, *et al*, "Seasonal and diurnal cycles of liquid water in snow—Measurements and modeling," *Journal of Geophysical Research: Earth Surface*, Vol. 120, No. 10, pp. 2139–2154, 2015.

[19] A. Godio, *et al*., "Seasonal monitoring of snow properties by WCR and up-GPR," *21st European Meeting of Environmental and Engineering Geophysics – Near Surface Geoscience 2015*, Turin, Italy, September 6–10, 2015.

[20] L.Schmid, F. Kock, A. Heilig, M. Prasch, O. Eisen, W. Mauser, and J. Schweizer, "A novel sensor combination (upGPR-GPS) to continuously and nondestructively derive snow cover properties," *Geophysical Research Letters*, Vol. 42, 2015.

[21] J. H. H. Eriksrød, J. F. Burkhart, T. S. Lande, and S. Hamran, "Bistatic SAR Radar for Long-Term Snow Pack Monitoring," *IEEE Transactions on Geoscience and Remote Sensing*, Vol. 58, No. 1, pp. 218-226, January 2020.

[22] B. Rekioua, M. Davy, L. Ferro-Famil, and S. Tebaldini, "Snowpack permittivity profile retrieval from tomographic SAR data," *Comptes Rendus Physique*, Vol. 18, pp. 57–65, 2017.

[23] K. Morrison and J. Bennett, "Tomographic Profiling—A Technique for Multi-Incidence-Angle Retrieval of the Vertical SAR Backscattering Profiles of Biogeophysical Targets," *IEEE Transactions on Geoscience and Remote Sensing*, Vol. 52, No. 2, pp. 1350–1355, 2014.

[24] Y. Yamaguchi, M. Mitsumoto, M. Sengoku, and T. Abe, "Synthetic aperture FM-CW radar applied to the detection of objects buried in snowpack," *IEEE Transactions on Geoscience and Remote Sensing*, Vol. 32, No. 1, pp. 11–18, 1994.

[25] W. S. Holbrook *et. al*., "Estimating snow water equivalent over long mountain transects using snowmobile-mounted ground-penetrating radar," *Geophysics*, Vol. 81, No. 1, pp. WA213–WA223, January-February 2016.

[26] N. Griessinger, F. Mohr, and T. Jonas, "Measuring snow ablation rates in alpine terrain with a mobile multioffset ground-penetrating radar system," *Hydrological Processes*, Vol. 32, pp. 3272–3282, October 2018.

[27] J. St. Clair and W. S. Holbrook, "Measuring snow water equivalent from common-offset GPR records through migration velocity analysis," *The ryosphere*, Vol. 11, pp. 2997–3009, December 2017.

[28] J. Brown, J. Harper, and N. Humphrey, "Liquid water content in ice estimated through a full-depth ground radar profile and borehole measurements in western Greenland," *The Cryosphere*, Vol. 11, pp. 669-679, 2017.

[29] J. Brown, J. Bradford, J. Harper, W. T. Pfeffer, N. Humphrey, and E. Mosley-Thompson, "Georadar-derived estimates of firn density in the percolation zone, western Greenland ice sheet," *Journal of Geophysical Research*, Vol. 117, 2012.

[30] J. Brown, J. Harper, W. T. Pfeffer, N. Humphrey, and J. Bradford, "High-resolution study of layering within the percolation and soaked facies of the Greenland ice sheet," *Annals of Glaciology*, Vol. 52, No. 59, 2011.

[31] J. H. Bradford, J. Nichols, T. D. Mikesell, and T. Harper, "Continuous profiles of electromagnetic wave velocity and water content in glaciers: an example from Bench Glacier, Alaska, USA," *Annals of Glaciology*, Vol. 50, No. 51, 2009.

[32] M. Pasian, M Barbolini, F. Dell'Acqua, P. F. Espín-López, and L. Silvestri, "Snowpack monitoring using a dual-receiver radar architecture," *IEEE Transactions on Geoscience and Remote Sensing*, Vol. 57, No. 2, pp. 1195–1204, 2019.

[33] P. F. Espín-López and M. Pasian, "Determination of snow water equivalent for dry snowpacks using the multipath propagation of ground-based radars," *IEEE Geoscience and Remote Sensing Letters*, Vol. 18, No. 2, pp. 276–280, February 2021.

[34] M. Pasian, P. F. Espín-López, L. Silvestri, M. Barbolini, and F. Dell'Acqua, "Experimental validationo of a dual-receiver radar architecture for snowpack monitoring," *EuMA International Journal of Microwave and Wireless Technologies*, Vol. 12, No. 6, pp. 439–446, July 2020.

[35] M. T. Hallikainen, F. T. Ulaby, and M. Abdelrazik, "Dielectric properties of snow in the 3 to 37 GHz range," *IEEE Transactions on Antennas and Propagation*, Vol. 34, No. 11, pp. 1329–1340, November 1986.

[36] J. H. Bradford, J. T. Harper, and J. Brown, "Complex dielectric permittivity measurements from ground-penetrating radar data to estimate snow liquid water content in the pendular regime," *Water Resource Research*, Vol. 45, 2009.

[37] M. A. Richards, J. A. Scheer, and W. A. Holm, *Principles of Modern Radar – Basic Principles*, SciTech Publishing, 2010.

[38] C. A. Balanis, *Antenna Theory*, Wiley, 2005.

[39] P. Pouliguen, R. Hemon, C. Bourlier, J. F. Damiens, and J. Saillard, "Analytical formulae for radar cross section of flat plates in near field and normal incidence," *Progress In Electromagnetic Research*, Vol. 9, pp. 263–279, 2008.

[40] A. H. Sihvola and M. E. Tiuri, "Snow fork for field determination of the density and wetness profiles of a snow pack," *IEEE Transactions on Geoscience and Remote Sensing*, Vol. 24, No. 5, pp. 717–721, 1986.

[41] F. Techel and C. Pielmeier, "Point observations of liquid water content in wet snow – investigating methodical, spatial and temporal aspects," *The Cryosphere*, Vol. 5, pp. 405–418, 2011.

[42] R. W. Webb, K. S. Jennings, M. Fend, and N. P. Molotch, "Combining ground-penetrating radar with terrestrial LiDAR scanning to estimate the spatial distribution of liquid water content in seasonal snowpacks," (2018).. *Water Resources Research*, Vol. 54, No. 12, pp. 10,339–10,349, December 2018.

[43] L. Quéno, C. Fierz, A. van Herwijnen, D. Longridge, and N. Wever, "Deep ice layer formation in an alpine snowpack: monitoring and modeling,", *The Cryosphere*, Vol. 14, pp. 3449–3464, 2020.

[44] H. Hirashima, F. Avanzi, and S. Yamaguchi, "Liquid water infiltration into a layered snowpack: evaluation of a 3-D water transport model with laboratory experiments," *Hydrology and Earth System Sciences*, Vol. 21, pp. 5503–5515, 2017.